RSC Advances

PAPER

View Article Online
View Journal | View Issue

Cite this: *RSC Adv.*, 2015, **5**, 7454

Au/Ag bimetal nanogap arrays with tunable morphologies for surface-enhanced Raman scattering

Yaxin Wang,[a] Xiaoyu Zhao,[a] Wenting Gao,[a] Lei Chen,[a] San Chen,[c] Maobin Wei,[a] Ming Gao,[a] Cong Wang,[a] Yongjun Zhang*[a] and Jinghai Yang*[ab]

Received 21st September 2014
Accepted 22nd December 2014

DOI: 10.1039/c4ra10882e

www.rsc.org/advances

When Au and Ag were deposited onto two-dimensional polystyrene (PS) templates, a curved bimetallic film composed of nanocap-shaped Au/Ag units was formed. The "Y"-shaped nanogaps and "V"-shaped junctions were tailored between the neighbour nanocaps by changing the bilayer thickness and PS diameters. Compared to the curved Ag, the curved Au monolayer and the flat Au/Ag bilayer on a silicon wafer, the curved Au/Ag bimetallic film exhibited significant SERS enhancement, which was mainly attributed to two important factors, the nanogaps between the adjacent Au/Ag nanocaps and the composite of the Ag/Au bimetallic film. And the nanogaps generated extremely intense local electromagnetic fields and the composite provided more possibilities for the residence of probing molecules.

1. Introduction

Surface-enhanced Raman scattering (SERS) observed in the 1970s is a phenomenon where a Raman signal is strongly enhanced when molecules are attached to the rough surface of metal nanostructures.[1,2] In recent years, a tremendous amount of studies have focused on SERS due to its single-molecule sensitivity and excellent fingerprint effect for practical applications in detection and recognition technology fields.[3–7] Currently, the development of patterned substrates with nanogap arrays is an important aspect of SERS studies, because the large electromagnetic (EM) fields can be excited at the nanogaps, termed as "hot spots", due to the surface plasmon resonances (SPR) of the nanostructure, which can significantly amplify Raman scattering intensity of the attached molecules.[8–10] A variety of nanostructures with "hot spots" have been fabricated by different approaches including chemical functionalization method,[11] electron lithography technique[12] and salt-induced aggregation.[13,14] In comparison, nanosphere lithography (NSL) is a simple, economic and robust route for the fabrication of a uniformly ordered nanostructure array owing to its good monodispersity, wide size range (nanometer-to-micrometer) and easy availability.[15–18]

In addition to the construction of the substrate with high density of hot spots, the material composition is another key factor for SERS enhancement. Generally, SERS-active substrates have been restricted to some noble metals materials.[19] Comparing with other noble metals, Ag and Au nanoparticles have been widely used in SERS studies due to the higher plasmonic enhancement for Ag and better biocompatibility for Au.[20,21] But the toxicity of Ag and weak SERS active of Au have limited the development of SERS spectroscopy for the application of the single metallic substrate. To optimize SERS effect and other optical properties, recently, a number of studies focus on some composites or bimetal materials system, including Au@SiO_2, Ag/ZnO.[22,23] Au/Ag bimetal system attracts tremendous attentions from the SERS community because it exhibits both the dramatic Raman enhancement and good compatibility.[24–27] The bimetal films composed of the Ag and Au are preferable choices for the enhancement of SERS signal and application in analytical technique.

In this work, we fabricate the SERS-active substrate composed of Au/Ag metallic nanogap array by NSL. The morphologies and the properties of the metallic nanogaps are modified by adjusting the PS diameter and the film thickness. The influences of the different morphologies and the compositions of Au/Ag on Raman effects are investigated.

2. Experimental section

Assemble of PS array

The monodisperse polystyrene colloid particles (PS) were purchased from Duke Cooperation (10 wt% aqueous solution). The diluted polystyrene solution was applied onto the modified

[a]*Key Laboratory of Functional Materials Physics and Chemistry, Jilin Normal University, Ministry of Education, Siping 136000, PR China. E-mail: zhangyongjunwyx@126.com; jhyang@jlnu.edu.cn*

[b]*Key Laboratory of Excited State Physics, Changchun Institute of Optics Fine Mechanics and Physics, Chinese Academy of Sciences, Changchun, 130033, PR China*

[c]*Huaibei Normal University, Huaibei, 235000, PR China*

substrate, which spread all over the substrate. The substrate was then slowly immersed into the glass vessel filled with water and the PS particles started to form an unordered monolayer on the water surface. The sodium dodecyl sulfate solution was added onto the water surface, which drove the monolayer into highly ordered pattern. The monolayer of the close-packed two-dimensional PS array was picked up by the decorated silicon substrate. The detailed process of the self-organization was reported in our previous jobs.[28] The plasma etching was performed to form two-dimensional array of separated PS. The etching process was performed in a plasma cleaner (Model 1020, E.A. Fischione Instruments Inc.), and the working gas was a mixture of 80% O_2 and 20% Ar.

Fabrication of Au/Ag nanocap array

The nanocap arrays of Au/Ag bilayer with different thickness were fabricated on PS array of different sizes in magnetron sputtering system (ATC 1800-F, USA AJA). The Au layer of different thickness first was deposited on PS then Ag layer was deposited on Au layer by dc sputtering Au target and Ag target respectively. The purities of Au target and Ag target are both 99.9999% and the sputtering power is both 40 W. The deposition rates of Au and Ag were 0.22 nm s^{-1} and 0.13 nm s^{-1} respectively. The base pressure was 2.0×10^4 Pa and the argon pressure was 0.6 Pa during film deposition. The distance between the target and substrate was 20 cm.

Fabrication of SERS substrate

The substrates of Au/Ag bilayer on PS were immersed in a 1 mM 4-mercaptopyridine (4-MPy) alcohol solution for 3 h, and were washed thoroughly for several minutes to remove unabsorbed 4-Mpy. The samples were finally dried in air for 20 min for the measurement of SERS. Raman spectra were measured using Renishaw inVia Raman system with a 514.5 nm Ar^+ ion laser excitation (2.41 eV, 20 mW). The Raman emissions, dispersed in a 0.5 m single monochromator equipped with a grating of 1800 grooves per cm, were detected with CCD. A 50 × 0.50 NA Leica object focused the excitation beam onto the samples with a spot diameter of *ca.* 1 μm. The signal acquisition time was 10 s in a 180° backscattering geometry. According to manufacturer specifications, the solid angle of collection Ω was 0.37 steradian.

Characterization of nanocap array

The morphology and microstructure of the bilayer arrays were investigated by scanning electron microscope (SEM, JEOL 6500F) and transmission electron microscope (TEM, 200 keV, JEM-2100HR). Ultraviolet-visible (UV-vis) absorption spectra were obtained on a Shimadzu UV-3600 spectrophotometer.

3. Results and discussions

Fig. 1 illustrates the fabrication process of Au/Ag bilayer nanocap arrays by NSL in a magnetic control sputtering system. The left column shows the schematic image and the SEM (or TEM) observations are shown in the right column. First, the

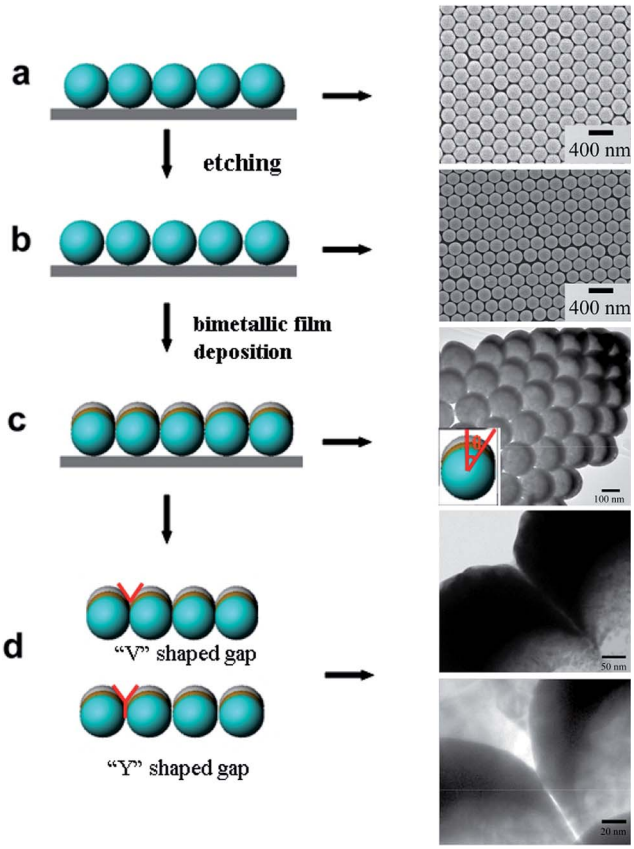

Fig. 1 The schematic, SEM and TEM images for the fabrication process of Au/Ag bilayer nanocaps arrays. (a) Close-packed PS array. (b) The separated PS arrays. (c) Au/Ag nanocap array on PS template. The inset is the schematic of film thickness for the bilayer on PS sphere surface. (d) "Y"-shaped nanogap and "V"-shaped junction.

monolayer two-dimensional (2D) PS arrays with different sizes are prepared on Si wafer by self-assembly method. The arrays form perfect ordered hexagonal arrangements on a large area, as shown in Fig. 1a. These close-packed PS are then etched for 20 s by plasma etching technique to create nanogaps between the adjacent PS beads. The adjacent PS beads are separated slightly and a large amount of nanogaps form (Fig. 1b). Subsequently, the Au layer is deposited onto the separated PS bead arrays, and then Ag layer is deposited onto Au layer to form Au/Ag bilayer (Fig. 1c). The TEM image in the right column shows that the film covers the top and sidewall of PS. When Au/Ag film is deposited onto the PS array, the film thickness decreases from the nanocap top to the brim. When the thickness is smaller than the PS radius, the variation of the thickness can be expressed by the equation $t(\theta) = t_0 \cos \theta$, where t_0 is the thickness of the film on the sphere top and θ is the angle with respect to the normal direction of the substrate (the inset). In this case, two kinds of morphologies may form, depending on the PS radius and the film thickness. When the film is thin, the separated nanocap arrays form, where many "Y"-shaped nanogaps exist between adjacent PS beads. When the film thickness is much larger than PS bead radius, the nanogaps disappear. The nanocaps are connected with each other and

the pseudo-continuous film structure forms with "V"-shaped junction between adjacent PS beads. The schematic of "Y"-shaped and "V"-shaped nanostructures and corresponding TEM images are shown in Fig. 1d.

Fig. 2 shows the UV-vis absorption spectra for different thickness Au (5 nm, 10 nm, 15 nm, 20 nm, 25 nm)/Ag (50 nm) bilayer on PS 200 nm array (Fig. 2a) and PS 500 nm array (Fig. 2b), respectively. For PS 200 nm (Fig. 2a), the absorption spectra show broadened band from around 400 nm to near-infrared area, which is caused by the excitation of surface plasmon resonances in Ag NPs, Au NPs, single semi-shells, and the dipole resonances among Ag–Ag NPs, Ag–Au NPs and semi-shells. Besides that, Au and Ag coated periodical PS array are also contributed to their broad absorbance. With the increase of Au content, the absorbances increase and a new red-shifted plasmonic absorption band appears around 520 nm, which indicates the formation of composite of Au and Ag. The red-shifted and broadened plasmon absorption bands are attributed to the localized plasmon coupling of Au NPs, Ag NPs and semi-shells.[29] For PS 500 nm (Fig. 2b), the band at around 400 nm is assigned to the absorption band of Ag NPs. Meanwhile, the absorption bands at around 520 nm and 600 nm can be assigned to the Au NPs and the dipole resonance between Au–Au and Au–Ag. The appearances of three significant bands for PS 500 nm indicate the SPR coupling effects between neighbour nanocaps are weakened due to the increase of PS bead size.

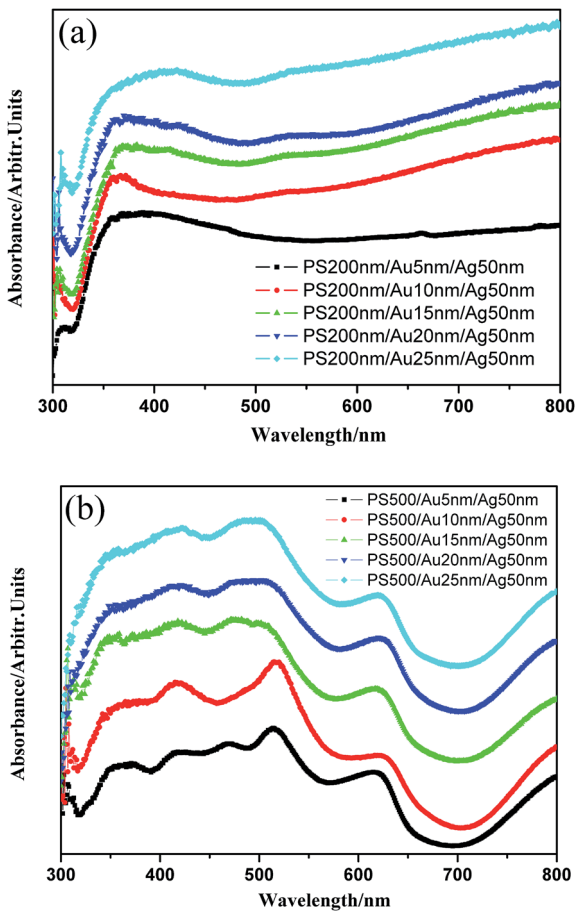

Fig. 2 UV-vis absorption spectra for different thickness Au (5 nm, 10 nm, 15 nm, 20 nm and 25 nm)/Ag (50 nm) bilayer on PS 200 nm (a) and 500 nm (b) array.

Fig. 3a–c shows the typical Raman spectrum of the 4-MPy absorbed on bimetal film Au (t nm)/Ag 50 nm (t = 5 nm, 10 nm, 15 nm, 20 nm, 25 nm, and 30 nm). The SERS peaks agree well with the findings reported in the literature.[30] The dominant peaks at 1604 cm^{-1} represent the aromatic C–C stretching vibrational mode, which are used to study the evolution of the peaks intensities with the bilayer thickness. Fig. 3d–f shows the dependences of the SERS intensity on Au thickness. The SERS signals increase first with Au layer thickness and then decreases, and the maximum count point reaches 10^5 for the Au 25 nm/Ag 50 nm on PS 200 nm array. The similar behaviors are observed for PS 100 nm and PS 500 nm arrays. The maximum values of SERS intensity are obtained for the bilayers Au 5 nm/Ag 50 nm on PS 100 nm and Au 50 nm/Ag 150 nm on PS 500 nm templates, respectively.

The nanogaps between adjacent nanocaps play a key role in the SERS enhancement. For PS 200 nm substrate (Fig. 3e), when the bilayer thickness is very thin, almost all material is deposited on the sphere top to form the nanocaps due to the change of bilayer thickness (inset in Fig. 3e). With the increase of the total film thickness, the nanocaps extend along the sphere surface and create sidewalls between adjacent PS beads, and the "Y"-shaped gaps considered as hot spots start to form, which enhances the SERS effect. When the total thickness increases further, the adjacent nanocaps are connected and the gaps disappear, and the morphology of the nanogaps changes gradually from "Y" shape to "V" shape. The Raman signal intensity starts to decrease. Compared to bilayer on PS 200 nm array, the decreases of nanogap density in the array are mainly responsible for the decrease of Raman signal intensity on PS 500 nm array (Fig. 3f). For the bilayer on PS 100 nm array (Fig. 3d), the SERS intensity decreases obviously when the total thickness is larger than 70 nm, which is attributed to the formation of "V"-shaped or pseudo-continuous film, reducing the SPR coupling effect from the nanogaps.

Fig. 4 shows the TEM images of Au 25 nm/Ag 50 nm bilayer deposited on PS 200 nm and PS 100 nm templates. For the bilayer on PS 200 nm array (Fig. 4a), the nanocaps are also in ordered pattern. The "Y"- shaped nanogap is observed clearly from the amplified inset and the size is about 3 nm (shown by arrows). These nanogaps confine and excite particularly large enhancements of the electromagnetic field, which is a desirable for the enhancement of local electrical field and SERS.[31] For Au/Ag bilayer on PS 100 nm template (Fig. 4b), the adjacent nanocaps are connected and the nanogaps disappear. The nanogap morphology changes from the "Y"-shaped gap to the "V"-shaped junction (shown by arrows) and leads to the declination of hot spots, which can directly be responsible for the decreased SERS intensity.

The composition of the Ag/Au bimetal material is another important factor for SERS enhancement. To investigate the influence of material composition on SERS enhancement, the Ag 75 nm and Au 75 nm monolayers are fabricated on PS

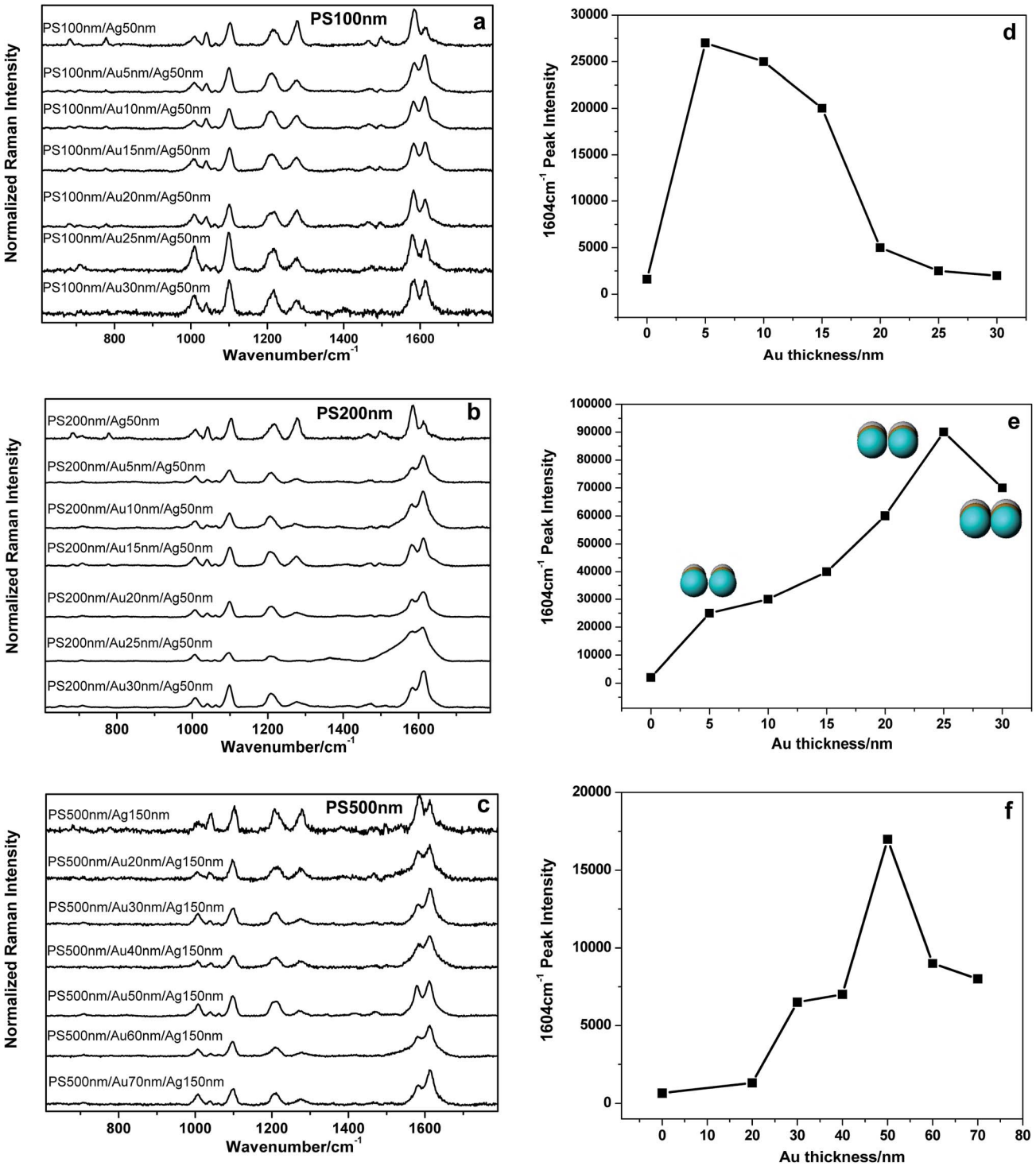

Fig. 3 The Raman spectrum of 4-MPy in a normalized form and the corresponding dependence of the Raman signal intensity on bilayer thickness for the different thickness Au/Ag bilayer array deposited on (a and d) 100 nm (b and e) 200 nm (c and f) 500 nm. The schematic in (e) shows the structure of nanocap on the adjacent nanospheres for different film thickness.

200 nm template. Compared to Au 25 nm/Ag 50 nm bilayer on PS 200 nm, the curved Ag 75 nm and Au 75 nm monolayer all exhibit very weak SERS signal (Fig. 5), and similar results are observed by other researchers.[32] The results indicate that the curved bilayer with Au and Ag composite can significantly improve SERS performance. SERS intensity on PS 100 exhibits the lower intensity of SERS than that on PS 200 nm, which is somewhat unexpected if we only consider the density of nanogap between adjacent nanocap as the bilayer on PS 100 have high density of nanogap than that on PS 200. Meanwhile, we

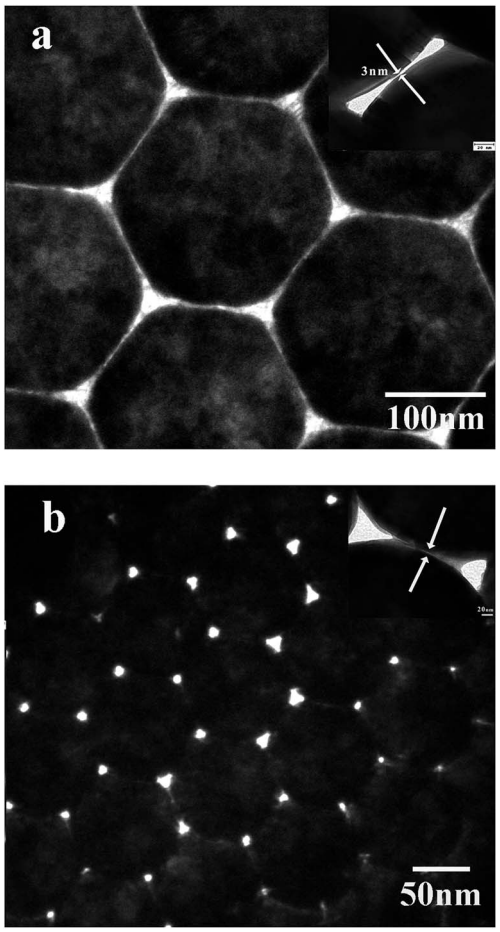

Fig. 4 TEM images of the Au 25 nm/Ag 50 nm bimetal nanocap array on (a) 200 nm (b) 100 nm PS template respectively. The inset shows the "Y"-shaped nanogap and "V"-shaped junction.

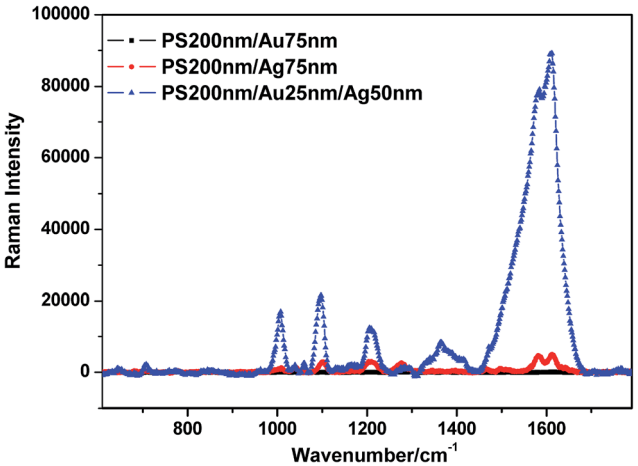

Fig. 5 SERS spectra of 1 mM 4-MPy on PS 200 nm/Au 75 nm, PS 200 nm/Ag 75 nm and PS 200 nm/Au 25 nm/Ag 50 nm respectively.

know that Au/Ag bilayer on PS surface tend to transform into AuAg monolayer composed of Au and Ag islands at the sidewall of each nanocap due to the decrease of film thickness. Some crevices will appear between Ag and Au islands, which provide more possibilities to trap analyte molecules in the crevices because of the high intrinsic SERS activity of Ag and the excellent compatibility of Au.[33,34] So the Au and Ag composites at sidewall also contribute to the enhancement of SERS besides the nanogaps between adjacent nanocaps. For the PS 100 nm array, the nanogap already disappear due to the smaller PS size when Au and Ag composition reach the proper ratio causing the maximum enhancement of SERS, which may be a important factor for SERS intensity of PS 100 nm lower than PS 200 nm.

When bilayer Au 25 nm/Ag 50 nm is deposited onto PS 200 nm template, the bilayer film transforms into the monolayer in the sidewall. And the inset shows the monolayer is composed of the discrete Au and Ag islands (Fig. 6). The line-scan EDS analysis is performed along the yellow line in TEM measurement and the results confirm the monolayer sidewall is composed of Ag (49.09 wt%) and Au (50.91 wt%).

To estimate the electromagnetic field distribution in the nanogap structure, the local EM field is calculated by the finite-difference time-domain (FDTD) method. Fig. 7 shows the typical top views of the calculated radial EM field for the nanocap array with "Y"-shaped and "V"-shaped gaps. The array is approximated by the fundamental nanostructure unit composed of seven hexagonally arranged spheres. The linearly polarized plane wave with 514 nm propagates along the normal of the sample surface, with electric field parallel to the sample surface. It is obvious that the strong field enhancement occurs in the "Y"-shaped and "V"-shaped regions under the normal incident. The stronger EM field concentrated in the "Y"-shaped nanogap than the "V"-shaped junctions which are known as hot spots for SERS enhancement.

The SERS enhancement factor (EF) is calculated by using $EF = (I_{SERS} \times N_{bulk})/(I_{bulk} \times N_{ads})$ to compare the Raman intensity of the 1604 cm^{-1} band,[35,36] where I_{SERS} and I_{bulk} are the SERS intensities for 4-MPy on the surface of nanocap array and the pure 4-MPy reference solution (10^{-3} M) respectively.

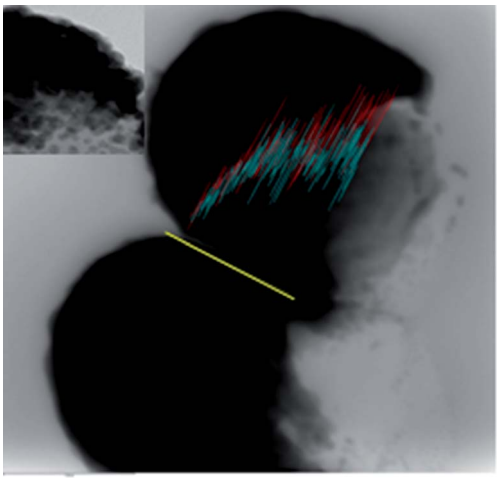

Fig. 6 TEM image shows the Au/Ag bimetal nanocap is composed of Au and Ag islands. EDS analysis (along the yellow line) shows the nanocap sidewall is composed of Ag (red line) and Au (cyan line).

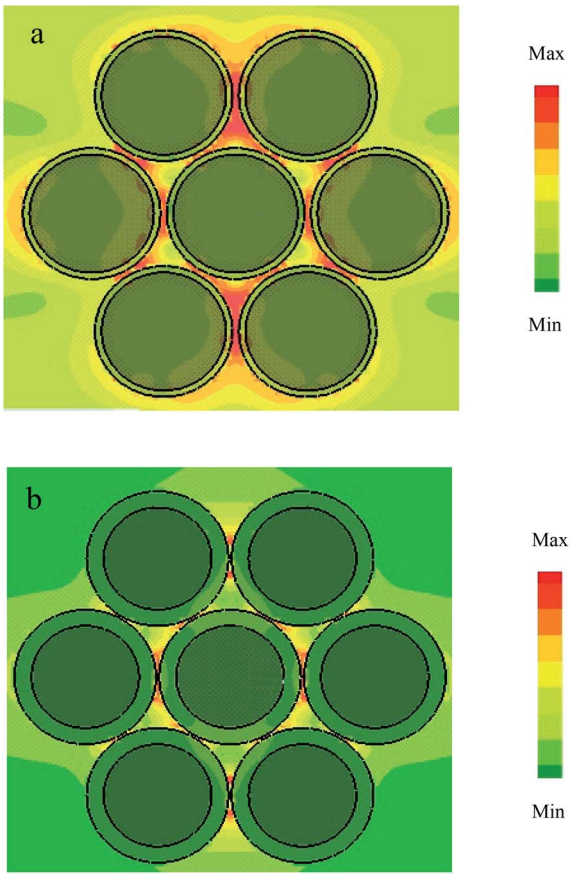

Fig. 7 E-field intensity distribution (indicated by the color bar) of nanogap array on PS 200 nm template for different morphologies. (a) "Y"-shaped gaps, (b) "V"-shaped junctions.

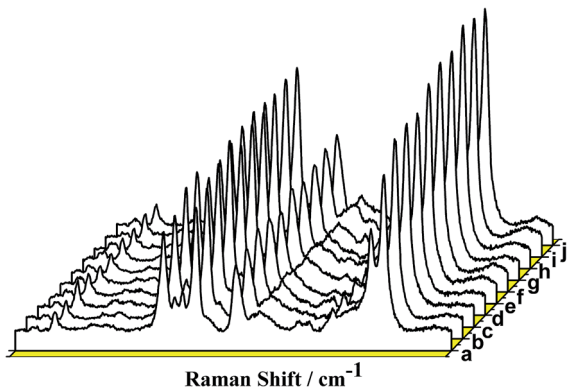

Fig. 8 SERS spectra of 4-MPy absorbed on bimetal PS 200 nm/Au 25 nm/Ag 50 nm bilayer at 10 random positions across a 4 cm^2 substrate.

$N_{bulk} = c_{RS}VN_A$ is the average number of molecules in the scattering volume (V) for the Raman (non-SERS) measurement. The molar concentration (c_{RS}) of the 4-MPy analyte on the reference region is 1 mM. N_{ads} is the average number of adsorbed molecules in the scattering volume for the SERS experiments. $N_{ads} = N_d A_{laser} A_N/\sigma$ where N_d is the number density of PS with diameter 200 nm, and A_{laser} is the area of the focal laser spot. A_N is the half surface area of one PS with diameter 200 nm, and σ is the surface area occupied by a single 4-MPy adsorbed molecule on the substrate value. The substrate is washed thoroughly for several times to remove unabsorbed 4-MPy after it is immersed into the 1 mM 4-MPy molecule aqueous solution for 3 h. And all free molecules are washed away. Only a thin layer molecule is left onto the substrate. Therefore, it is assumed that 4-MPy forms a monolayer on the substrate and the surface area occupied by single 4-MPy molecules is estimated to be 0.30 nm.[2,37] In our experiment, the spot of laser is a circle with a diameter of 1 μm, and the effective focused depth is 19 μm. N_{bulk} and N_{ads} can be calculated to be 9.69×10^{13} and 5.24×10^6, respectively. The value of I_{SERS}/I_{bulk} is 0.9×10^3 for Au 25 nm/Ag 50 nm substrate and 50 for Ag 75 nm substrate. So the EF is calculated to be 1.66×10^9 for Au 25 nm/Ag 50 nm nanocaps substrate and 9.20×10^7 for Ag substrate, respectively.

We study the reproducibility of SERS substrate for the bimetal on PS 200 by measuring random spots across the whole nanocap array. Fig. 8 shows the SERS spectra collected from 10 random positions across a 4 cm^2 substrate. The maximum standard deviation of the intensity is calculated to be 11.2% with respect to the average intensity of the band at 1060 cm^{-1}, indicating the SERS enhancements are uniform across the sample surface. The homogenous and high-ordered Au/Ag bimetal nanocap arrays provide a promising application in biosensor and quantitative analysis of spectroscopy.

4. Conclusion

In conclusion, Au/Ag bimetal nanogaps arrays induced by curved spherical surface were successfully fabricated by depositing Au/Ag film onto two-dimensional PS colloidal nanosphere template. The different morphologies with "Y"-shaped nanogaps and "V"-shaped junctions formed by changing the film thickness and the nanosphere diameters. Both the experimental spectra and the simulation of the electric-field distribution showed a prominent SERS enhancement at "Y"-shaped or "V"-shaped nanogaps, which were mainly attributed to the combined effects of the nanogaps between the adjacent nanocaps and the composite formation of Au and Ag islands in the bilayer nanocap.

Acknowledgements

This work is supported byProgram for the development of Science and Technology of Jilin province (no. 20120359, 20140519003JH, 20150519024JH and 20150520015JH), Program for the master students' scientific and innovative research of Jilin Normal University (no. 201109).

References

1 M. G. Albrecht and J. A. Creighton, *J. Am. Chem. Soc.*, 1977, **99**, 5215–5217.

2 D. L. Jeanmaire and D. Van, *J. Electroanal. Chem.*, 1977, **84**, 1–20.
3 T. Brule, H. Yockell-Lelievre, A. Bouhelier, J. Margueritat, L. Markey, A. Leray, A. Dereux and E. Finot, *J. Phys. Chem. C*, 2014, **118**, 17975–17982.
4 J. F. Li, Y. F. Huang, Y. Ding, Z. L. Yang, S. B. Li, X. S. Zhou, F. R. Fan, W. Zhang, Z. Y. Zhou, D. Y. Wu, B. Ren, Z. L. Wang and Z. Q. Tian, *Nature*, 2010, **464**, 392–395.
5 X. M. Qian, X. H. Peng, D. O. Ansari, Q. Yin Goen, G. Z. Chen, D. M. Shin, L. Yang, A. N. Young, M. D. Wang and S. M. Nie, *Nat. Biotechnol.*, 2007, **26**, 83–90.
6 B. Peng, G. Y. Li, D. H. Li, S. Dodson, Q. Zhang, J. Zhang, Y. H. Lee, H. V. Demir, X. Y. Ling and Q. H. Xiong, *ACS Nano*, 2013, **7**, 5993–6000.
7 R. Zhang, Y. Zhang, Z. C. Dong, S. Jiang, C. Zhang, L. G. Chen, L. Zhang, Y. Liao, J. Aizpurua, Y. Luo and J. L. Yang, *Nature*, 2013, **498**, 82–86.
8 G. Braun, I. Pavel, A. R. Morrill, D. S. Seferos, G. C. Bazan, N. O. Reich and M. Moskovits, *J. Am. Chem. Soc.*, 2007, **129**, 7760–7761.
9 H. Im, K. C. Bantz, S. H. Lee, T. W. Johnson, C. L. Haynes and S. H. Oh, *Adv. Mater.*, 2013, **25**, 2678–2685.
10 K. Kim, J. Y. Choi and K. S. Shin, *J. Phys. Chem. C*, 2013, **117**, 11421–11427.
11 G. Chen, Y. Wang, M. Yang, J. Xu, S. J. Goh, M. Pan and H. Chen, *J. Am. Chem. Soc.*, 2010, **132**, 3644–3645.
12 N. A. Hatab, C. H. Hsueh, A. L. Gaddis, S. T. Retterer, J. H. Li, G. Eres, Z. Zhang and B. Gu, *Nano Lett.*, 2010, **10**, 4952–4955.
13 W. Li, P. H. C. Camargo, X. Lu and Y. Xia, *Nano Lett.*, 2009, **9**, 485–490.
14 J. P. Camden, J. A. Dieringer, Y. Wang, D. J. Masiello, L. D. Marks, G. C. Schatz and D. Van, *J. Am. Chem. Soc.*, 2008, **130**, 12616–12617.
15 X. L. Li, Y. Z. Zhang, Z. X. Shen and H. J. Fan, *Small*, 2012, **8**, 2548–2554.
16 G. Sriram, A. K. Shadak, C. Andrea and F. Maurizio, *J. Appl. Phys.*, 2012, **112**, 084303.
17 A. D. McFarland, M. A. Young, J. A. Dieringer and R. V. Duyne, *J. Phys. Chem. B*, 2005, **109**, 11279–11285.
18 D. A. Stuart, J. M. Yuen, N. Shah, O. C. R. Lyandres, M. R. Glucksberg, J. T. Walsh and R. V. Duyn, *Anal. Chem.*, 2006, **78**, 7211–7215.
19 X. Y. Hu, G. W. Meng, Q. Huang, W. Xu, F. M. Han, K. X. Sun, Q. L. Xu and Z. M. Wang, *Nanotechnology*, 2012, **23**, 385705.
20 K. Hyelim, J. H. Chul, C. J. Hwan, Y. L. Su and M. Y. Seung, *ACS Appl. Mater. Interfaces*, 2013, **5**, 4569–4574.
21 Y. B. Zheng, J. L. Payton, T. B. Song, B. K. Pathem, Y. Zhao, H. Ma, Y. Yang, L. Jensen, K. Y. Jen and P. S. Weiss, *Nano Lett.*, 2012, **12**, 5362–5368.
22 V. Varadee, M. V. Brandon, W. B. William, H. K. Jun and T. R. Lee, *ACS Appl. Mater. Interfaces*, 2011, **3**, 3616–3624.
23 X. He, H. Wang, Z. B. Li, D. Chen and Q. Zhang, *J. Mater. Chem.*, 2012, **22**, 7902–7909.
24 J. Zhu, J. J. Li, L. Yuan and J. W. Zhao, *J. Phys. Chem. C*, 2012, **116**, 11734–11740.
25 Y. Zhou, C. W. Lee, J. N. Zhang and P. Zhang, *J. Mater. Chem. C*, 2013, **1**, 3695–3699.
26 M. K. Fan, F. J. Lai, H. L. Chou, W. T. Lu, B. J. Hwang and A. G. Brolo, *Chem. Sci.*, 2013, **4**, 509–515.
27 B. Chen, G. W. Meng, Q. Huang, Z. L. Huang, Q. L. Xu, C. H. Zhu, Y. W. Qian and Y. Ding, *ACS Appl. Mater. Interfaces*, 2014, **18**, 15667–15675.
28 Y. J. Zhang, W. Li, J. Li, Y. M. Zhang, Y. X. Wang, S. Y. Yang and S. S. Liu, *J. Appl. Phys.*, 2012, **111**, 053925.
29 J. Q. Tang, Q. H. Zhang, C. Y. Zeng and S. Q. Man, *Appl. Phys. A*, 2013, **111**, 1099–1105.
30 C. X. Wang, W. D. Ruan, N. Ji, W. Ji, S. Lv, C. Zhao and B. Zhao, *J. Phys. Chem. C*, 2010, **114**, 2886–2890.
31 T. Hutter, S. R. Elliott and S. Mahajan, *Nanotechnology*, 2013, **24**, 035201.
32 J. Stropp, G. Trachta, G. Brehm and S. Schneider, *J. Raman Spectrosc.*, 2003, **34**, 26–32.
33 Z. L. Huang, G. W. Meng, Q. Huang, Y. J. Yang, C. H. Zhu and C. L. Tang, *Adv. Mater.*, 2010, **22**, 4136–4139.
34 K. Kim, D. H. Shin, K. L. Kim and K. S. Shin, *Phys. Chem.*, 2010, **12**, 3747.
35 B. Ren, X. F. Lin, Z. L. Yang, G. K. Liu, R. F. Aroca, B. W. Mao and Z. Q. Tian, *J. Am. Chem. Soc.*, 2003, **125**, 9598–9599.
36 P. He, H. T. Liu, Z. Y. Li, Y. Liu, X. D. Xu and J. H. Li, *Langmuir*, 2004, **20**, 10260–10267.
37 W. B. Cai, B. Ren, X. Q. Li, C. X. She, F. M. Liu, X. W. Cai and Z. Q. Tian, *Surf. Sci.*, 1998, **406**, 9–22.

